Monte Carlo Simulation of Kinetics and Chain Length Distributions in Living Free-Radical Polymerization

Junpo He,† Hongdong Zhang,† Jingming Chen,† and Yuliang Yang*,†,‡

Department of Macromolecular Science, Lab of Macromolecular Engineering, SEDC, Fudan University, Shanghai 200433, China, and Institute of Chemistry, Academia Sinica, Beijing 100080, China

Received October 7, 1996; Revised Manuscript Received September 8, 1997[⊗]

ABSTRACT: The kinetics and chain length distributions occurring in living free-radical polymerizations are simulated using a hybrid Monte Carlo algorithm. The new algorithm is much faster than the conventional one because the activation/deactivation exchange reactions, which are CPU intensive, are treated by a biased-sampling method with an analytical expression for the exchange equilibrium, while the reactions of chain propagation, irreversible chain termination, etc. are treated by exact stochastic Monte Carlo simulation. Two models of living radical polymerizations, i.e., the polymerization initiated by alkoxyamines and the nitroxide radical, 2,2,6,6-tetramethyl-1-piperidinyloxy, mediated radical polymerization, are simulated to study the effects of experimental variables, such as the concentration ratio of stable free radicals to initiators, initiation rate constants, etc., on the kinetics and molecular weight distributions. A comparison between simulated and analytical results in the literature is made. Taking thermal initiation into consideration, the algorithm reproduces the experimental results very well. Therefore, its feasibility and usefulness in studying living free-radical polymerization are demonstrated.

1. Introduction

Living free-radical polymerization (LFRP) has recently attracted much attention because it may avoid the weaknesses of ionic polymerization, in which high-purity monomers and solvents and anhydrous conditions are necessarily required, as well as the shortcomings of conventional free-radical polymerization, in which broad polydisperse products are inherently produced.[1−9] The earlier works were focused on the livingness, i.e., the molecular weight of the resulting polymers increasing stepwise with monomer conversion, of free-radical polymerization initiated by iniferters (*ini*tiator−trans*fer* agent−*ter*minator) such as disulfides or dithiocarbamates.[4,6,9] Lately, another initiating system, in which a stable free radical (SFR) such as 2,2,6,6-tetramethyl-1-piperidinyloxy (TEMPO) plays the role of chain-end trapper, has been developed for LFRP to prepare polymers with narrow molecular weight distributions (MWDs).[2,7,10,11] However, very slow polymerization rates inhibit the application of these systems on a large scale. In order to improve LFRPs, it is necessary to understand their reaction mechanisms. Following the kinetic analysis of group transfer polymerization (GTP) by Muller et al.,[12] Veregin studied the dependence of MWDs on monomer conversion in TEMPO-mediated LFRP[13] and compared them with experimental results. However, to simplify the mathematics, the initiation of polymerization was assumed to be very rapid and irreversible chain termination was ignored in the analytical analysis.

On the other hand, computer modeling and numerical solution of the large number of differential kinetic equations of LFRP have been used to interpret the kinetics and MWDs found experimentally.[14−16] However, these methods suffer from the need for a supercomputer, which is not often available to most research teams. Besides that, in principle, the MWDs and the kinetics of LFRPs should be described by an infinite number of differential equations. One has to truncate the infinite-sized simultaneous differential equation set somewhere, by artificially introducing the "closure reaction".[17] In ref 14, a system of up to 500 differential equations has been used in the computation. This artificial truncation will make the calculated MWD and polydispersity index, d, unreliable when some of the chains are longer than 500, a problem noticed by Johnson et al.[14] Therefore, both the accuracy and monomer conversion one can reach are limited by the number of differential kinetic equations used in the computation, which, in turn, is limited by available computer memory and CPU performance. Recently, the stochastic Monte Carlo algorithm[18] has proven to be a useful technique for studying the kinetics and MWDs in free-radical polymerization.[19,20] The convenience and feasibility of the stochastic Monte Carlo algorithm have been demonstrated when it has been used for pulsed laser, or rotating sector, initiated radical polymerization, with or without chain transfer reactions.[19,20] This algorithm has also been extended to simulate bulk multifunctional free-radical polymerization in which the kinetic constants are diffusion-dependent.[21]

In this paper, our purposes are to apply the Monte Carlo algorithm to LFRP after improving the method, to study the effects of several experimental variables, such as the SFR/initiator ratio, rate constants, etc., on kinetics and MWDs in two simple models of LFRPs, and to compare our results with those from the analytical method, as well as those from experimental observations. Finally, some differences in results are discussed.

2. Model Description

A number of LFRP schemes have been reported elsewhere.[22] In general, there are two kinds of LFRP systems that can be defined in two models.

* To whom the correspondence should be addressed.
† Fudan University.
‡ Academia Sinica.
⊗ Abstract published in *Advance ACS Abstracts,* November 15, 1997.

S0024-9297(96)01485-4 CCC: $14.00

Model I

$$\mathrm{SR}(j) \underset{k_{-\mathrm{f}}}{\overset{k_{\mathrm{f}}}{\rightleftharpoons}} \mathrm{S} + \mathrm{R}(j) \qquad j = 1, 2, ..., j_{\max}$$

activation/deactivation exchange between growing and dormant chains

$$\mathrm{R}(j) + \mathrm{M} \xrightarrow{k_{\mathrm{p}}} \mathrm{R}(j+1) \qquad \text{chain propagation}$$

$$\mathrm{R}(i) + \mathrm{R}(j) \xrightarrow{k_{\mathrm{t}}} \mathrm{P}(i) + \mathrm{P}(j) \quad \text{or} \quad \mathrm{P}(i+j)$$

irreversible chain termination

In this kinetic model, R(j) is a growing radical with chain length j (when j = 1, R(j) represents chain initiation), M is a monomer, P(j) is a dead polymer with chain length j, and S is a stable free radical (SFR) such as TEMPO, which can deactivate (to form dormant chains SR(j)) and activate (to form growing chains R(j) and S) chain ends reversibly but cannot initiate polymerization by itself. It is evident that the possibility of biradical termination to form dead polymers will be greatly reduced because of the equilibrium between the growing chain radicals and the stable radicals. The decomposition of the initiator, SR(1), is not explicitly shown. For simplicity, chain transfer reactions are ignored because they are only important when transfer agents are added. Moreover, of combination and disproportionation irreversible chain termination, only the latter is considered. One exception is that, in section 4.6, when compared to the experimental data quantitatively, the combination irreversible chain termination is considered, and the following side reactions are added:[15,16]

Thermal initiation

$$\mathrm{M} + \mathrm{M} \xrightarrow{k_{\mathrm{dim}}} \mathrm{D}$$

$$\mathrm{D} + \mathrm{M} \xrightarrow{k'_{\mathrm{i}}} \mathrm{R}(2) + \mathrm{R}(1)$$

Thermal decomposition of the dormant chains

$$\mathrm{SR}(j) \xrightarrow{k_{\mathrm{decomp}}} \mathrm{P}(j) + \mathrm{SH}$$

where D is an unsaturated dimer and SH is a hydroxylamine-type molecule.

Model II. The disadvantage of model I is that one has to synthesize the specific initiators that can release SFRs during initiation. In experiment, two-component initiating systems are often used to initiate LFRP (e.g., AIBN/TEMPO or BPO/TEMPO initiated styrene polymerization,[3] in which SFR is in excess from the beginning). This model can be given by adding the homolytic cleavage of initiators

$$\mathrm{I} \xrightarrow{k_{\mathrm{d}}} 2\mathrm{R}(0)$$

to the reaction scheme of model I. Here, for simplicity, we ignore the difference between primary radicals and chain radicals.

3. Monte Carlo Algorithm

3.1. Basic Algorithm. Our previous simulation algorithm for free radical polymerization[19,20] is based on Gillespie's master equation.[18] The details of the algorithm were given in ref 19. In order to keep the integrity of this paper, here we briefly review this algorithm.

Suppose the volume V contains a spatially homogeneous mixture of X_l molecules of chemical species A_l (l = 1, 2, ..., N) and these N species can interact through M specified chemical reaction channels R_μ (μ = 1, 2, ..., M). The kind of reaction μ that will happen in a time interval ($t \rightarrow t + \tau$) is determined by a unit-interval uniformly distributed random number, r_1, according to the following relation:

$$\sum_{\nu=1}^{\mu-1} R_\nu < r_1 \sum_{\nu=1}^{M} R_\nu \le \sum_{\nu=1}^{\mu} R_\nu \tag{1}$$

where R_ν is the rate of νth reaction. For a bimolecular second-order reaction, R_ν can be generally written as

$$R_\nu = k_{lm} X_l X_m \tag{2}$$

where k_{lm} is the microscopic reaction rate constant in Monte Carlo simulation and X_l and X_m are the number of molecules of species (reactants) l and m in the system, respectively. The reaction probability of reaction channel n is defined as

$$P_\nu = \frac{R_\nu}{\sum_{\nu=1}^{M} R_\nu} \tag{3}$$

and it satisfies the relation

$$\sum_{\nu=1}^{M} P_\nu = 1 \tag{4}$$

The Monte Carlo rate constants, k^{MC}, are microscopic and can be transformed into macroscopic experimental constants, k^{exp}, according to the following relations (when the experimental concentration is defined as moles per unit volume):[23]

$$k^{\mathrm{MC}} = k^{\mathrm{exp}} \qquad \text{for first-order reactions} \tag{5}$$

$$k^{\mathrm{MC}} = \frac{k^{\mathrm{exp}}}{VN_{\mathrm{a}}} \qquad \text{for bimolecular reactions between different species}$$

$$k^{\mathrm{MC}} = \frac{2k^{\mathrm{exp}}}{VN_{\mathrm{a}}} \qquad \text{for bimolecular reactions between indistinguishable species} \tag{6}$$

where N_{a} is Avogadro's constant and V is the total volume of the reaction system (V can be eliminated by the initial mole concentration of one kind of reactant, e.g., $[\mathrm{B}]_0$, through the definition of mole concentration, $VN_{\mathrm{a}} = X_{\mathrm{B}}^0[\mathrm{B}]_0$, with X_{B}^0 as the initial number of molecules of species B used in the Monte Carlo simulation). Using the above process, the simulated results are given in real time scale and can be directly compared with the experimental results.[19,23,24]

In the exact stochastic simulation, the time interval between two successive reactions, τ, is a stochastic variable determined by a unit-interval, uniformly distributed random number, r_2 ,

$$\tau = \frac{1}{\sum_{\nu=1}^{M} R_\nu} \ln\left(\frac{1}{r_2}\right) \tag{7}$$

3.2. Improvement of the Algorithm. Although the above algorithm effectively simulates conventional free-radical polymerizations, it is very slow when applied to LFRPs. By carefully looking at the simulation process, we find that the reaction probabilities of activation/deactivation exchange are much greater than the probabilities of other reactions. This can be easily checked by comparison of the reaction rates of various reaction channels:

$$R_p = k_p[M]\sum_j R(j) \approx 2 \times 10^2 \times 1 \times 10^{-7} = 2 \times 10^{-5}$$

$$R_t = k_t(\sum_j R(j))^2 \approx 5 \times 10^6 \times 10^{-14} = 5 \times 10^{-8}$$

$$R_f = k_f\sum_j SR(j) \approx 1 \times 10^{-1} \times 10^{-3} = 10^{-4}$$

$$R_{-f} = k_{-f}[S]\sum_j R(j) \approx 1 \times 10^8 \times 10^{-7} = 10^{-3}$$

where we have assumed that [M] = 1 (mol/L), the total concentration of radicals is 10^{-7} (mol/L), and [S] is 10^{-4} (mol/L). The rate constants are the same as those we used in most of our simulations shown below. It is clearly seen that the reaction probability of a reversible exchange reaction channel is at least 100 times greater than all other reaction channels. Therefore, large amounts of CPU time would be spent on reversible activation/deactivation exchange reaction channels such as SR(j) ↔ R(j) + S in LFRP models. This is a special characteristic found only in LFRPs as opposed to conventional radical polymerizations. However, this reversible exchange reaction does not affect measurable quantities, such as the MWDs and the concentration of monomer, etc. To improve efficiency, a hybrid model is used for the simulation of SFRP. We assume that, in a time interval ($t \rightarrow t + \tau$), the equilibrium of the reversible reactions has been established. Under this assumption, instead of random sampling, the reversible reactions are treated analytically; i.e., the number of molecules of all species that participate in the reversible reaction, at given evolution time $t + \tau$, can be calculated according to the following equation:

$$\frac{X_S(t+\tau)\sum_j X_{R(j)}(t+\tau)}{\sum_j X_{SR(j)}(t+\tau)} = \frac{(X_S(t)+\Delta)(\sum_j X_{R(j)}(t)+\Delta)}{\sum_j X_{SR(j)}(t)-\Delta} = \frac{k_f^{MC}}{k_{-f}^{MC}} = K_{eq} \quad (8)$$

$X_l(t)$ and $X_l(t+\tau)$ are the number of molecules of species l at time t and $t + \tau$, respectively. Due to the biradical irreversible termination reaction, which consumes growing radicals, the equilibrium at time t is lost. To reestablish equilibrium at time $t + \tau$, the number of molecules should be adjusted by Δ. A potential problem is that Δ, calculated by eq 8, is generally not an integer. However, the noninteger value of Δ can be safely replaced by its integer value because the error introduced by this replacement is less than ±0.5. Futhermore, because the error in each step is randomly distributed in the range of ±0.5, the statistical error in the whole simulation can theoretically be eliminated. After the number of molecules is readjusted according to the integer value of Δ, the newly formed growing radicals, R(j), are randomly selected from all the molecules of SR(j), j = 1, 2,.... The newly formed dormant chains, SR(i), however, are randomly selected from all the growing radicals R(i), i = 1, 2, ... Thus, the activation/deactivation exchange reaction channels can all be merged into an equilibrium reaction channel R_{eq},

$$R_{eq} = R_f + R_{-f} = k_f\sum_j SR(j) + k_{-f}[S]\sum_j R(i) \quad (9)$$

This improved algorithm can be considered a hybrid of analytical and stochastic algorithms. The above reversible exchange reaction channel is treated analytically, while the other reaction channels are treated stochastically. However, large amounts of CPU time still must be spent on the reversible exchange reaction channel due to the very large reaction probability of R_{eq} compared to that of R_p and R_t. In order to solve this problem in our simulation, we adopted a biased sampling method. In the biased sampling method the reaction probabilities can be weighted as follows to match P_p and P_t with P_{eq} in model I

$$P'_p = \frac{cR_p}{c(R_p + R_t) + R_{eq}}$$

$$P'_t = \frac{cR_t}{c(R_p + R_t) + R_{eq}}$$

$$P'_{eq} = \frac{R_{eq}}{c(R_p + R_t) + R_{eq}} \quad (10)$$

and in model II

$$P'_d = \frac{cR_d}{c(R_p + R_t + R_d) + R_{eq}}$$

$$P'_p = \frac{cR_p}{c(R_p + R_t + R_d) + R_{eq}}$$

$$P'_t = \frac{cR_t}{c(R_p + R_t + R_d) + R_{eq}}$$

$$P'_{eq} = \frac{R_{eq}}{c(R_p + R_t + R_d) + R_{eq}} \quad (11)$$

In eqs 10 and 11, c is an arbitrary constant set at 100, which means that the reaction channels of R_p, R_t, and R_d have been artificially multiplied 100 times. This artificially biased sampling should be corrected and compensated for in later calculations. The kind of reaction, μ, which will happen is determined by a unit-interval, uniformly distributed random number, r_1, according to the following modified relation:

$$\sum_{\nu=1}^{\mu-1} P_\nu' < r_1 \le \sum_{\nu=1}^{\mu} P_\nu' \quad (12)$$

If decomposition, propagation, or termination takes place, time interval t can also be calculated by eq 7. Once a reversible reaction takes place, the correction and compensation for the biased sampling should be done. The reversible exchange reaction should run c times in the time interval $t \rightarrow t + \tau$. This will

compensate for the artificial reduction of the probabilities of the reversible exchange channel. The time interval for the c successive reactions, τ', should be calculated by the following coarse-grained relation:

$$\tau' = \frac{c}{\sum_{\nu=1}^{M} R_\nu} \ln\left(\frac{1}{r_2}\right) \tag{13}$$

Since we have assumed that the equilibrium among the reversible exchange reactions have been established during the time interval τ', instead of running the equilibrium reactions c times, we simply solve eq 8 once to obtain Δ. The number of molecules are then readjusted according to the integer value of Δ. Using this method, simulation time is substantially reduced.

The general principle of above-mentioned improvement can be applied to any other chemical system, in which there is a great difference in magnitude among the reaction probabilities of various reaction channels. What one needs is that those large probabilities, which are otherwise CPU intensive, can be described by well-defined analytical expressions.

The simulation algorithms are coded in NDP FORTRAN and performed on an IBM-PC 486-50 MHz. The typical CPU time, using the improved algorithm, for the simulation of the monomer conversion up to 90%, is approximately 20 h. This is at least 40 times faster than the nonimproved algorithm. The results obtained from the improved algorithm have been checked by comparing them with those obtained by the nonimproved one. (For the comparison, please refer to the figure captions.)

In this simulation, the initial number of monomers is 10^9. This is assumed to be 1.0 mol/L. $[SR]_0$ is 1.0×10^{-3} mol/L for model I; $[I]_0 = 1.0 \times 10^{-3}$ mol/L for model II, if there is no further notation. The propagation and termination rate constants, k_p and k_t, are set at 2×10^2 and 5×10^6 L/(mol·s), respectively. The k_p/k_t ratio is $\sim 4 \times 10^{-5}$, approximately the same as the value of methyl methacrylate at 60 °C. The deactivating rate constant of the chain end by a stable radical, k_{-f}, is 10^8 L/(mol·s), approximately the same as the value of alkoxydi-*tert*-butylamine.[14,17] To simplify the procedure, all the rate constants are assumed to be independent of chain length. In addition, the efficiencies of initiation are assumed to be 100%.

4. Simulation Results and Discussion

4.1. General Features of LFRP. We would first like to look at the general features of the simplest LFRP (model I) obtained from our simulation and to compare these features with the results obtained from conventional free-radical polymerization. The polymerization scheme of the conventional free-radical polymerization is similar to model II, but without SFR. The rate constant, k_f, in LFRP is set at 1.0×10^{-1} s^{-1} ($K_{eq} = k_f/k_{-f} = 1.0 \times 10^{-9}$ mol/L), and k_d, in conventional radical polymerization, is assumed to be 5.0×10^{-5} s^{-1}. This is approximately the same as the decomposition rate constants of peroxide or diazo compounds. The values of k_p and k_t are given in the last section and are the same for both polymerization processes.

The most apparent difference between conventional and living radical polymerization lies in the dependence of MWDs on monomer conversion. As shown in Figure 1, the average chain length (thereby molecular weight) increases linearly with monomer conversion in LFRP

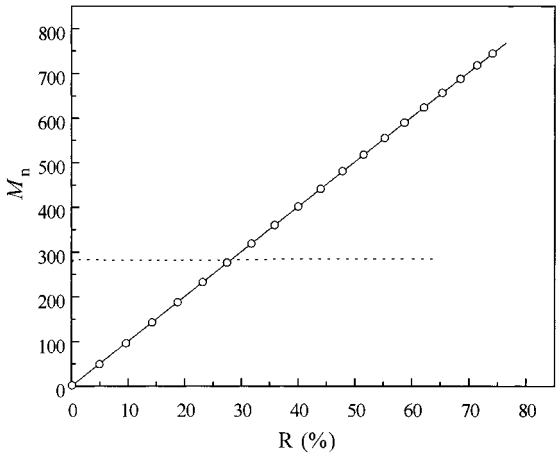

Figure 1. Average chain lengths $\bar{M}_n$ as a function of monomer conversion for model I of LFRP (solid line) and conventional radical polymerization (dotted line). For LFRP, the solid line is obtained by using our improved algorithm and the open circles are obtained by using the conventional Monte Carlo algorithm. In our simulation, $[M]_0 = 1$ mol/L, $[SR]_0 = 10^{-3}$ mol/L, $k_p = 2.0 \times 10^2$ L/(mol·s), $k_t = 5.0 \times 10^6$ L/(mol·s), $k_f = 1.0 \times 10^{-1}$ s^{-1}, and $k_{-f} = 1.0 \times 10^8$ L/(mol·s) for model I of LFRP and $k_d = 5.0 \times 10^{-5}$ s^{-1}, and $[I]_0 = 10^{-3}$ mol/L for conventional radical polymerization.

while it remains constant in conventional free-radical polymerization (after an initial sharp increase, which is not shown in Figure 1). The stepwise growth of molecular weight has been observed experimentally for various SFR-mediated polymerizations.[2,3,25,26] Furthermore, for a living system, the MWDs are narrower,[27] and the peaks of the MWDs shift to higher values in line with monomer conversion (Figure 2). In contrast, the MWDs for conventional radical polymerization remain almost unchanged with monomer conversion. At the beginning of LFRP, due to the homolytic dissociation of initiator SRs in model I, the concentration of growing radicals increases sharply with monomer conversion. The concentration of growing radicals then slowly reaches a steady value after a brief decrease, while the concentration of SFR increases steadily (Figure 3). In the early stage, a relatively higher concentration of growing radicals, produced by decomposition of initiators, gives rise to a higher rate of irreversible termination and results in a higher value of d. After parts of the growing radicals have been irreversibly terminated, SFRs are in excess and suppress the irreversible termination. Consequently, a large part of the chains are able to survive the polymerization process as living chains (including growing and dormant chains). This survival of living chains is responsible for the decrease in the d value after the initial stage (Figure 4).

The biradical termination cannot be ignored completely in LFRP. It is, therefore, interesting to inspect the MWDs and polydispersities of growing and dead chains separately. In Figures 4 and 5, the MWDs and polydispersities for growing and dead chains in SFRP *vs* conversion are shown. The MWDs for dead polymers are much broader than those of living polymers because the dead polymers that are formed at different monomer conversions have quite different lengths. Figure 6 shows the percentage of dead polymers *vs* monomer conversion. The percentage of dead polymer is lower than 10%, even for 80% conversion. Therefore, it only slightly affects the MWD of the whole system under the simulation conditions.

4.2. Effect of the Dynamics of Activation/Deactivation. The dynamics of the activation and deactiva-

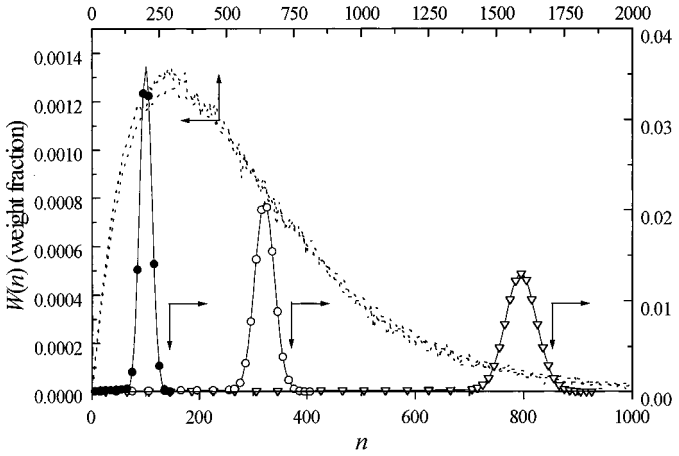

Figure 2. Weight fraction distributions for model I living (solid lines) and conventional (dotted lines) radical polymerizations at different monomer conversions indicated in the figure. The conversions for solid lines (from left to right) are 6.2%, 24.9%, and 49.8% and for dashed lines (from top to bottom) are 9.5%, 29.5%, and 69.4%, respectively. For the sake of comparison, the symbols are the results obtained for LFRP by using the conventional Monte Carlo algorithm. All the other parameters are the same as those of Figure 1.

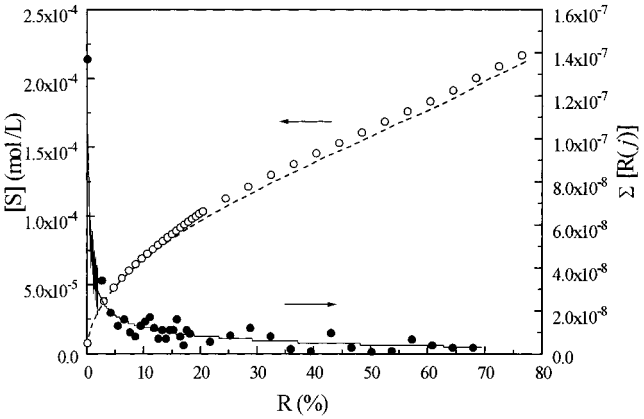

Figure 3. Concentrations of S (dotted line) and growing radicals (solid line) for model I of LFRP as a function of monomer conversion. The symbols are the data obtained using the conventional algorithm. All the parameters are the same as those of Figure 1.

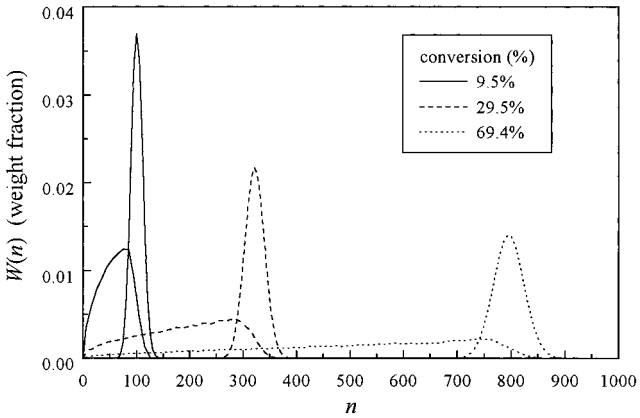

Figure 5. Weight fraction distributions of dead chains (lower ones) and living chains (including dormant chains) (upper ones). The weight fraction distributions of dead polymers and living chains are normalized separately. The parameters are the same as those in Figure 1.

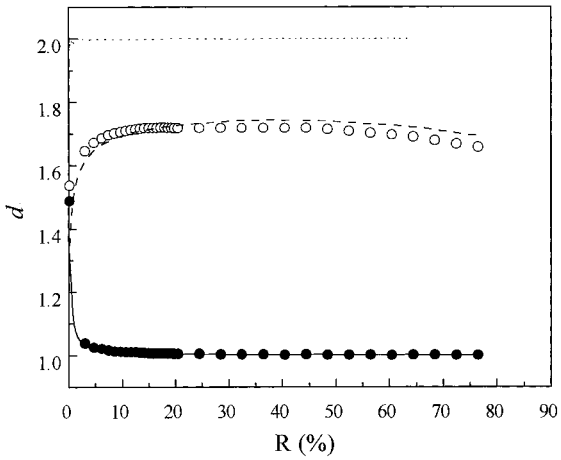

Figure 4. Polydispersity *d* for dead chains (dashed line) and living chains (including dormant chains) (solid line) in model I of LFRP and in conventional radical polymerization (dotted line) as a function of monomer conversion. The symbols and the parameters are the same as those in Figure 1.

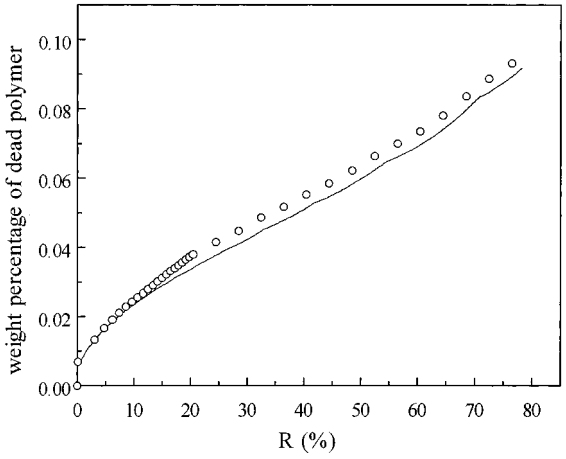

Figure 6. Weight percentage of dead chains for model I LFRP as a function of conversion. The solid line is the result obtained by our improved algorithm, while the symbols are the results of the conventional algorithm. All the parameters are the same as those in Figure 1.

tion exchange will have a strong effect on the polymerization rate and the MWD, as one would expect. To improve the LFRPs, the dynamics of exchange should be enhanced and the initiation accelerated (as pointed out by Greszta et al.[1]). This can be accomplished by a more facile homolytic cleavage (higher k_f) and by a simultaneous shift of the equilibrium to a low stationary concentration of growing radicals with an excess of SFRs. We believe that simultaneous enhancement of both k_f and k_{-f} (therefore the same K_{eq}) will have a

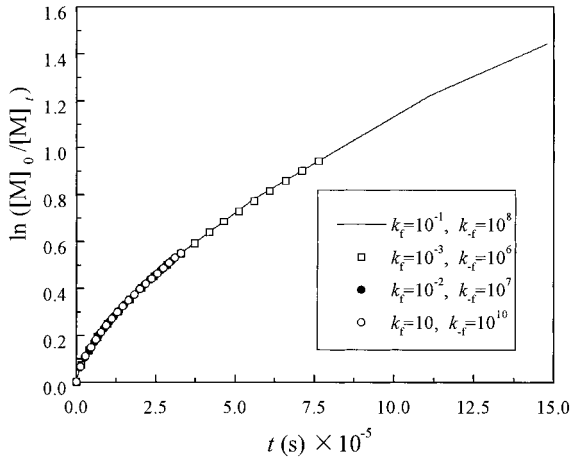

Figure 7. Plot of $\ln([M]_0/[M]_t)$ *vs* time for model I LFRP with different activation−deactivation exchange rate constants. All the other parameters are given in Figure 1.

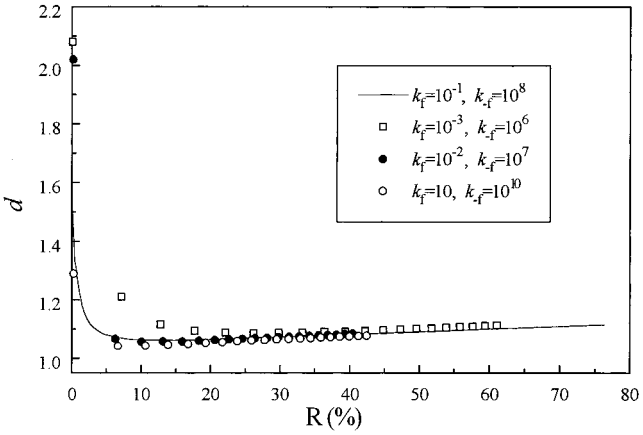

Figure 8. Polydispersity index, d, as a function of conversion for model I LFRP with different activation−deactivation exchange rate constants. The symbols and the solid line are the same as those of Figure 7, and all the other parameters are given in Figure 1.

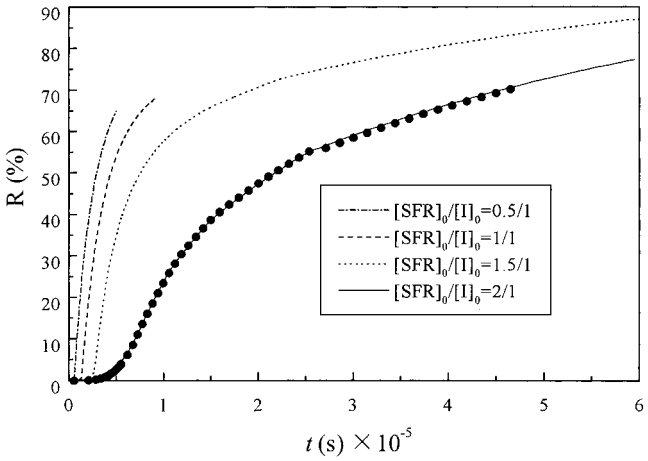

Figure 9. Plots of conversion *vs* time for model II LFRP with various values of $[SFR]_0/[I]_0$. The lines are results obtained from our improved algorithm, and the symbols are results obtained using the conventional algorithm. In this result, $[M]_0 = 5$ mol/L, $[I]_0 = 2.5 \times 10^{-3}$ mol/L, and $k_d = 5.0 \times 10^{-5}$ s^{-1}. All the other parameters are the same as those of Figure 1.

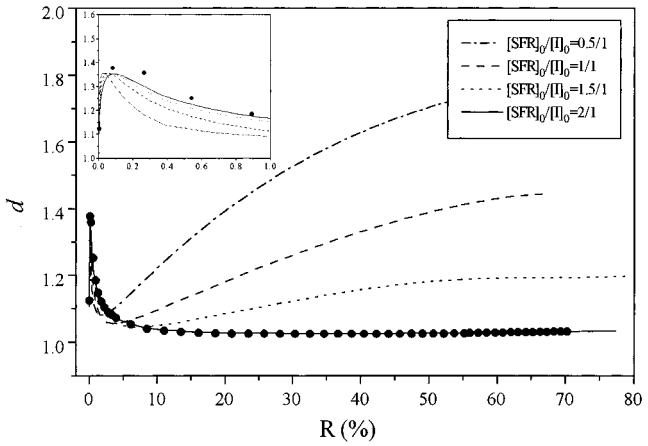

Figure 10. Plots of polydispersity index, d, *vs* conversion for model II of LFRP with various values of $[SFR]_0/[I]_0$. The symbols and parameters are the same as that of Figure 9. The insert window is an enlargement of the small conversion.

similar effect as above and keep the same low stationary concentration of growing radicals. We set $k_f = 1.0 \times 10^{-3}$−1.0×10^1 s^{-1} and $k_{-f} = 10^6$−10^{10} L/(mol·s) while keeping K_{eq} equal to 1.0×10^{-9} mol/L. (It should be mentioned here that the exact stochastic algorithm, not the hybrid one, has been used to avoid violation of the fast equilibrium assumption in the improved algorithm.) The results are shown in Figures 7 and 8. The polymerization rates and polydispersities at a high conversion are essentially unchanged. Only the polydispersities at a lower conversion show a slightly higher value for a slow exchange rate. Therefore, given our experimental conditions, LFRP cannot be substantially improved by increasing homolytic cleavage (higher k_f) and simultaneously keeping the same low stationary concentration of growing radicals.

4.3. General Behaviors of Model II. Now we turn to the case of model II, which is usually applied in experiments (e.g., AIBN/TEMPO- or BPO/TEMPO-initiated styrene polymerization[28,29]). The initial monomer concentration is set to $[M]_0 = 5$ mol/L. All the other rate constants are the same as those in model I.

The results show three characteristics of model II. First, the original ratio of stable radicals to initiators, $[SFR]_0/[I]_0$, has a strong effect on the polymerization rate. A lower value of $[SFR]_0/[I]_0$ gives rise to a faster polymerization rate (Figure 9) because the concentration of growing radicals is higher during the reaction time. Second, during the early stage of the reaction, there is an induction period (which was also observed in the experiment[3,28,29]). This can be attributed to the competition between trapping and propagation reactions of growing radicals during this period. At the beginning, large amounts of excess SFRs result in a much higher value of R_{-f} compared with R_p. When the reaction proceeds and TEMPO is consumed, R_{-f} is decreased and propagation begins, ending the induction period. As expected, a higher value of $[SFR]_0/[I]_0$ results in a longer induction period. Third, the polydispersity index, d, changes with monomer conversion. During the induction period, SFRs are in large excess, biradical termination can, therefore, be ignored, and d remains low. As the initiation process proceeds, the number of growing radicals, thus the probability of biradical termination reaction, increases. As a result, d increases and reaches a maximum (Figure 10, insert). Once the induction period is nearly complete, the polymerization rate increases quickly and the irreversible biradical termination reaction reduces the number of growing radicals to a steady value. The [SFR]/[R] ratio is, therefore, increased further. This ratio increase is responsible for the decrease in d after the induction period ends. On

the other hand, the residual initiators in the system still initiate polymerization, and the irreversible termination is still in progress. This seems responsible for the gradual increase in d at higher monomer conversion. However, the increase in d is very sensitive to the initial ratio of $[SFR]_0/[I]_0$. Once $[SFR]_0/[I]_0 \geq 2$, the increase in d disappears. This suggests that, under certain reaction conditions, the initial ratio of $[SFR]_0/[I]_0$ should be large enough to avoid the final increase in d. However, it should be pointed out that polymerization usually does not occur when $[SFR]_0/[I]_0$ is very high.

4.4. Effect of k_d and Comparison between Model II and Model I. In conventional free-radical polymerization, the decomposition rate of the initiator will strongly affect the kinetics of polymerization. In order to study its effect on LFRP in model II, we have simulated the polymerization processes of model II by setting $k_d = 5.0 \times 10^{-5}$, 1.0×10^{-4}, and 5.0×10^{-4} s^{-1}, respectively. For comparison, we keep $[I]_0 = 2.5 \times 10^{-3}$ mol/L, $[SFR]_0/[I]_0 = 2$ in model II, $[SR]_0 = 5 \times 10^{-3}$ mol/L in model I, and $[M]_0 = 5$ mol/L in the two models, and all the other rate constants are the same as before.

The results of conversion *vs* reaction time, t, for various k_d values, and their comparison with model I are shown in Figure 11. The conversion curves of model II approach those of model I at high monomer conversion, no matter whether the induction period exists or not. As k_d increases, the induction period shortens and the conversion curve approaches that of model I much earlier. Model I can be regarded as an extreme example of model II, with so large a k_d that initiation is completed at a very early stage. The changes in polydispersities d, and average chain lengths with monomer conversion are similar between model I and model II, given various k_d values.

4.5. Comparison with Analytical Results. Muller et al.[12] considered the degenerate transfer between active and dormant chain ends in group transfer polymerization (GTP). As GTP's key polymerization steps are quite similar to those of LFRP, Muller's results can be extended to study the MWDs in LFRP, mediated by nitroxide radicals.[13] The analytical expression obtained for the polydispersity is

$$d = \frac{1}{\gamma x} + \frac{1}{x}\left[2 + \frac{\beta - 1}{\alpha - \beta}(2 - x)\right] - \frac{2\alpha(1-\alpha)}{(\beta^2 - \alpha^2)x^2}[1 - (1-x)^{1+\beta/\alpha}] \quad (14)$$

where x is monomer conversion, $\alpha = [R]/[SR]$ with $[R] = ([SR]K_{eq})^{1/2}$ and SR the total number of TEMPO-terminated chains, $\beta = k_{-f}[S]/k_p[SR]$, and $\gamma = [M]_0/[SR]$. As the irreversible termination was not considered in the theoretical model of eq 14, the values of α, β, and γ become constant during the polymerization process after a very short initial stage (a few seconds). For the system with $[M]_0 = 1$mol/L, $k_f = 10^{-3}$ s^{-1}, and $k_{-f} = 10^6$ L/(mol·s), the results of exact stochastic simulation, without irreversible termination, and those of eq 14 are compared in Figure 12. The results are very similar. However, as already noticed by Muller et al.,[12] eq 14 includes residual initiators that are not a part of the polymer and, in experimental determination of the MWD, will not be measured. We feel that the contribution of the residual initiator should be extracted from the MWD. Therefore, we believe that the comparison between the experimental results and eq 14, made by Veregin et al.[13] is not very reliable. The polydispersity,

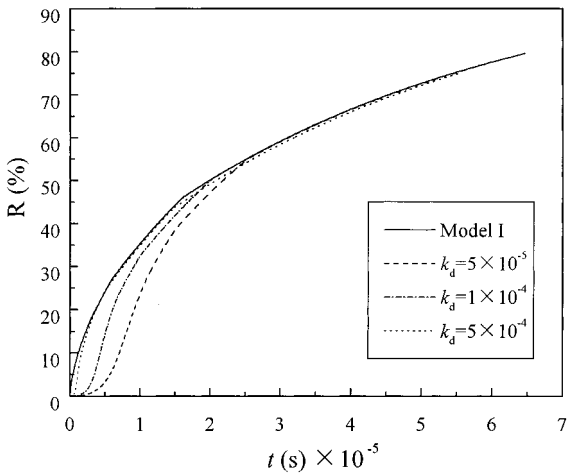

Figure 11. Plots of conversion *vs* time for model I (solid line) and model II (other lines) LFRPs with $[M]_0 = 5$ mol/L. For the sake of comparison, in model I $[SR]_0$ is set to be 5.0×10^{-3} mol/L, in model II $[I]_0 = 2.5 \times 10^{-3}$ mol/L and $[SFR]_0/[I]_0 = 2$. It can be seen that as k_d increases, the lines for model II are approaching the solid line of model I. All the other parameters are the same as in Figure 1.

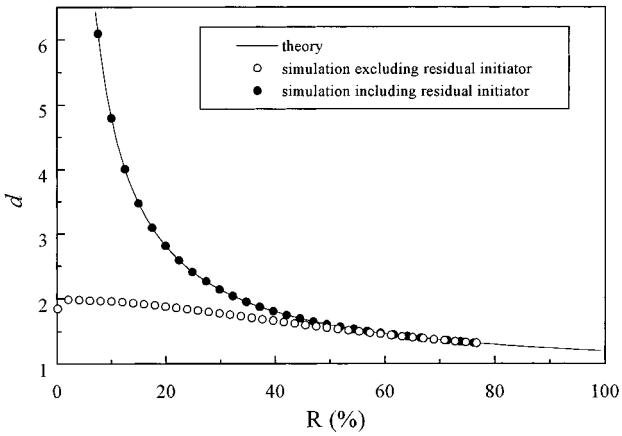

Figure 12. Plots of polydispersity index, d, *vs* conversion for theory and simulation based on the approach of slow equilibrium between growing and dormant chains. Dotted line, solid circles, and open circles, represent the theoretical results calculated by eq 14 and the simulation results including and excluding unreacted residual initiator, respectively. Here, $[M]_0 = 1$ mol/L, $[SR]_0 = 10^{-3}$ mol/L, $k_f = 10^{-3}$ s^{-1}, and $k_{-f} = 10^6$ L/(mol·s), hence, $\alpha = 0.001$, $\beta = 5$, and $\gamma = 1000$.

d, obtained after the residual initiator has been excluded, is much lower than that of eq 14, when $x < 30\%$, as shown in Figure 12. This agrees with the numerical results of Muller et al.[12]

4.6. Comparison with Experimental Results. Catala et al.[26] reported kinetic studies of styrene polymerization mediated by SR-type initiators, alkoxyamines, and found that the polymerization rate is independent of the initial concentration of SR in the range 3.7×10^{-3} to 4.4×10^{-2} mol/L. Recently, using the program PREDICI, Matyjaszewski et al.[15,16] simulated LFRP and attributed this phenomenon to the presence of self-initiated thermal styrene polymerization and thermal decomposition of alkoxyamines (as shown in our description of model I with the rate constants: $k_{dim} = 1.5 \times 10^{-9}$ L/(mol·s), $k_i' = 4.5 \times 10^{-9}$ L/(mol·s), and $k_{decomp} = 8 \times 10^{-6}$ s^{-1}).

In the Monte Carlo algorithm, it is easy to include these side reactions in LFRP. In adopting the above side reaction scheme proposed by Matyjaszewski,[16] we assumed that k_{dim}, k_i', and k_{decomp} are not as large as

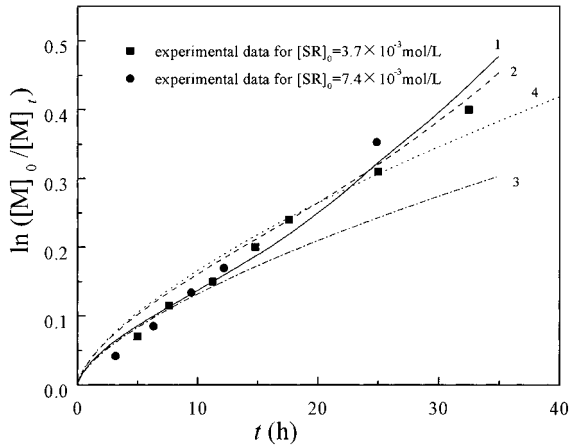

Figure 13. Dependence of $\ln([M]_0/[M]_t)$ *vs* time for bulk polymerization of styrene at 90 °C. Curves 1 and 2 represent simulated polymerization with thermal polymerization for $[SR]_0 = 3.7 \times 10^{-3}$ and 7.4×10^{-3} mol/L, respectively; curves 3 and 4 represent simulated polymerization without thermal polymerization for $[SR]_0 = 3.7 \times 10^{-3}$ and 7.4×10^{-3} mol/L, respectively. Key: (closed squares) experimental data for $[SR]_0 = 3.7 \times 10^{-3}$ mol/L; (closed circles) experimental data for $[SR]_0 = 7.4 \times 10^{-3}$ mol/L. The parameters are $[M]_0 = 8.75$ mol/L, $k_f = 2.5 \times 10^{-3}$ s^{-1}, $k_{-f} = 2.5 \times 10^{8}$ L/(mol·s), $k_p = 950$ L/(mol·s), $k_t = 10^7$ L/(mol·s), $k_{dim} = 1.5 \times 10^{-9}$ L/(mol·s), $k_i' = 4.5 \times 10^{-9}$ L/(mol·s), and $k_{decomp} = 8 \times 10^{-6}$ s^{-1}.

those assumed by Matyjaszewski.[16] The thermal polymerization rate in Catala's experiment (90 °C), therefore, should be smaller than that in Matyjaszewski's calculation (120 °C). Other rate constants, obtained as experimental data[26] ($[M]_0 = 8.75$ mol/L, $k_p = 950$ L/(mol·s), $k_t = 10^7$ L/(mol·s), $k_f = 2.5 \times 10^{-3}$ s^{-1}, $k_{-f} = 2.5 \times 10^8$ L/(mol·s), hence $K_{eq} = k_f/k_{-f} = 10^{-11}$ mol/L) are almost identical to Matyjaszewski's.[15,16] Using the rate constants given above, the experimental data can be fitted to the simulation curve quite well.

Figure 13 illustrates the simulated kinetic results of LFRP with and without thermal polymerization. In the absence of thermal polymerization, the plots of kinetic curves, with various initial SR concentrations, are very different. However, in the presence of thermal polymerization, it is evident that the plots of kinetic curves, with various initial SR concentrations, are almost identical to the experimental plots reported by Catala,[26] and also agree with Matyjaszewski's calculation.[15]

It is already known that the absence or presence of self-initiated thermal polymerization only leads to relatively small changes of polydispersities.[16] However, we proved, from our simulation results, that the thermal decomposition of the dormant chains, SR(j), does increase the polydispersities while it has almost no effect on monomer consumption. In Figure 14, by taking into account the thermal decomposition reaction of SR, the predicted polydispersities are much closer to those observed in experiment.

Figure 15 illustrates the evolution of molecular weights for the LFRP systems given various initial SR concentrations. Monte Carlo results, with or without side reactions, for the most part agree with Catala's report.[26] It seems that thermal polymerization and decomposition of SR have almost no effect on the evolution of molecular weights.

5. Conclusions

In summary, all typical experimentally observed phenomena of LFRPs can be reproduced by Monte Carlo simulations. The universal applicability of the Monte

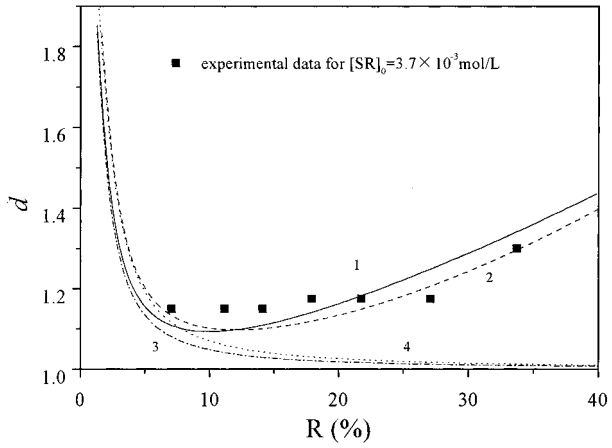

Figure 14. Dependence of polydispersities, d, on conversion for bulk polymerization of styrene at 90 °C. The lines and the parameters are the same as those in Figure 13. Closed squares are experimental data for $[SR]_0 = 3.7 \times 10^{-3}$ mol/L.

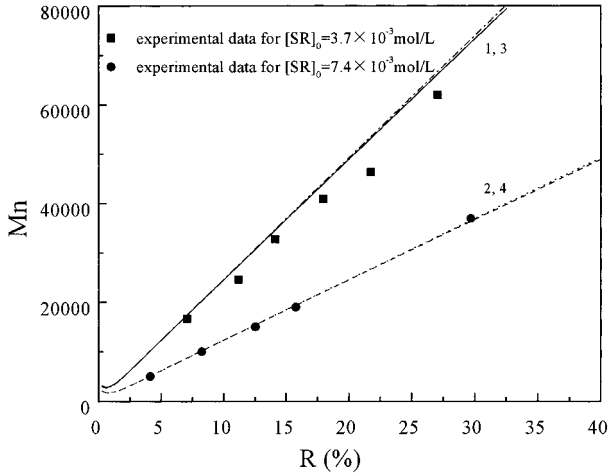

Figure 15. Dependence of number-averaged molecular weight on conversion for the bulk polymerization of styrene at 90 °C. The lines, symbols, and parameters are the same as those in Figure 13.

Carlo algorithm to LFRPs has been demonstrated. The most important advantage of using this algorithm is that it provides detailed information about the kinetics and MWDs, of both living and dead chains, varying with reaction time or monomer conversion in LFRP. The algorithm is also quite flexible in that various side reactions can be included in simulations. Through the study of the simplest LFRP models we have found the following.

(1) Using more facile homolytic cleavage (higher k_f) and simultaneously enhancing k_f (to keep the same low stationary concentration of growing radicals) may not accelerate LFRPs when the livingness of the polymerization is not altered.

(2) A higher k_d is needed to accelerate model II of LFRP during the early stages.

(3) The simulation results agree with the analytical expressions of polydispersity obtained by Muller et al.[12] (We also point out that unreacted residual initiators should be extracted from eq 14 when one desires to compare these results with those obtained from experiments.)

(4) Comparisons with experimental results indicate that thermal self-initiation and the thermal decomposition of SR are important to quantitatively reproduce experimentally observed behaviors.

In this study we have only dealt with the simplest LFRP models. We have not considered the possible effects of chain-length-dependent, or conversion-dependent rate constants, because of the lack of experimental data available. It is, however, not difficult to implement these effects in the present simulation program. Nevertheless, we believe that the results obtained from this simulation will be helpful for understanding the nature of LFRP, and for providing ideas for further experiments.

Acknowledgment. The authors truly appreciate the financial support from the NSF of China, the Qiu Shi Foundation of Hong Kong, and The Commission on Science and Technology of the Shanghai Municipality.

References and Notes

(1) Greszta, D.; Mardare, D.; Matyjaszewski, K. *Macromolecules* **1994**, *27*, 638.
(2) Mardare, D.; Matyjaszewski, K. *Macromolecules* **1994**, *27*, 645.
(3) Veregin, R. P. N.; Georges, M. K.; Hamer, G. K.; Kazmaier, P. M. *Macromolecules* **1995**, *28*, 4391.
(4) Lambrinos, P.; Tardi, M.; Ploton, A.; Sigwalt, P. *Eur. Polym. J.* **1990**, *26*, 1125.
(5) Bledzki, A. *Makromol. Chem.* **1983**, *184*, 745.
(6) Otsu, T.; Yamashita, K.; Tsuda, K. *Macromolecules* **1986**, *19*, 287.
(7) Nair, C. P. R.; Clouet, G.; Brossas, J. *J. Macromol. Sci., Chem.* **1988**, *A25*, 1089.
(8) Nair, C. P. R.; Clouet, G. *Polymer* **1988**, *29*, 1909.
(9) Otsu, T.; Matsunaga, T.; Kuriyama, A.; Yoshioka, M. *Eur. Polym. J.* **1989**, *25*, 643.
(10) Georges, M. K.; Veregin, R. P. N.; Kazmaier, P. M.; Hamer, G. K. *TRIP* **1994**, *2*, 66.
(11) Li, I.; Howell, B. A.; Matyjaszewski, K.; Shigemoto, T.; Smith, P. B.; Priddy, D. B. *Macromolecules* **1995**, *28*, 6692.
(12) Muller, A. H. E.; Zhang, R.; Yan, D.; Litvinenko, G. *Macromolecules* **1995**, *28*, 4326.
(13) Veregin, R. P. N.; Odell, P. G.; Michalak, L. M.; Georges, M. K. *Macromolecules* **1996**, *29*, 3346.
(14) Johnson, C. H. J.; Moad, G.; Solomon, D. H.; Spuring, T. H.; Vearing, D. J. *Aust. J. Chem.* **1990**, *43*, 1215.
(15) Greszta, D.; Matyjaszewski, K. *Macromolecules* **1996**, *29*, 5239.
(16) Greszta, D.; Matyjaszewski, K. *Polym. Prepr. (Am. Chem. Soc., Div. Polym. Chem.)* **1996**, *37* (2), 519.
(17) Johnson, C. H. J.; Moad, G.; Spuring, T. H.; Solomon, D. H. *Aust. J. Chem.* **1986**, *39*, 1943.
(18) Gillespie, D. T. *J. Phys. Chem.* **1979**, *81*, 2340.
(19) Lu, J.; Zhang, H.; Yang, Y. *Makromol. Chem., Theory Simul.* **1993**, *2*, 747.
(20) He, J.; Zhang, H.; Yang, Y. *Macromol. Theory Simul.* **1995**, *4*, 811.
(21) Kurdikar, D. L.; Somvarsky, J.; Dusek, K.; Peppas, N. A. *Macromolecules* **1995**, *28*, 5910.
(22) Eastmond, G. C. In *Comprehensive Chemical Kinetics*; Bamford, C. H., Tipper, C. F. H., Eds.; American Elsevier: New York, 1976; Vol. 14A.
(23) Lu, J.; Sun, M.; Yang, Y. *Chin. J. Polym. Sci.* **1994**, No. 5, 565.
(24) Yang, Y.; Zhang, H. *Monte Carlo Methods in Polymer Science* (in Chinese); Fudan University Press: Shanghai, 1993; p 240.
(25) Ivan, B. *Makromol. Chem., Macromol. Symp.* **1993**, *67*, 311.
(26) Catala, J. M.; Bubel, F.; Hammouch, S. O. *Macromolecules* **1995**, *28*, 8441.
(27) Odian, G. G. In *Principles of Polymerization*; John Wiley & Sons: New York, 1981.
(28) Georges, M. K.; Veregin, R. P. N.; Kazmaier, P. K.; Hamer, G. K. *Macromolecules* **1993**, *26*, 2987.
(29) Veregin, R. P. N.; Georges, M. K.; Kazmaier, P. K.; Hamer, G. K. *Macromolecules* **1993**, *26*, 5316.

MA9614858